MHD FLOW OF A REACTING AND RADIATING NANOLIQUID PAST AN INCLINED HEATED PERMEABLE PLATE: ANALYSIS OF ENTROPY GENERATION

O.D. MAKINDE† and A.S. EEGUNJOBI‡

† *Faculty of Military Science, Stellenbosch University, Private Bag X2, Saldanha 7395, South Africa.*
‡ *Mathematics Department, Namibia University of Science and Technology, Windhoek, Namibia*
Corresponding author: Samdet1@yahoo.com.

***Abstract*-- This paper examines the aggregate impacts of magnetic field, thermophoresis, Brownian motion, variable viscosity, chemical reaction and radiative heat flux on the thermal putrefaction and immanent irreversibility of a channelling nanoliquid film flowing along with a slanted heated permeable plate. Following the Buongiorno approach, the two-phase nanoliquid nonlinear model is obtained and addressed numerically using the shooting technique as well as the Runge-Kutta- Fehlberg integration scheme. Effects of various emerging parameters on the overall flow structure with heat and mass transfer characteristics including entropy generation rate and Bejan number are displayed using diagrams and discussed. It is found that the entropy generation rate lessened with an upsurge in a magnetic field but heightened with an elevation in the buoyancy forces.**

***Keywords*--MHD; Reactive nanoliquid; Inclined permeable plate; Variable viscosity; Convective cooling; Thermal radiation; Entropy analysis**

I. INTRODUCTION

Magnetohydrodynamics (MHD) flow of an electrically transferring nanoliquid past a slanted heated plate under the action of a transversely magnetic field has fascinated the interest of many researchers due to its application in geophysical, petroleum, boundary layer control in aerodynamics, sterilizing devices, oil recovery, thermal engineering and industries. Choi (1995) was the first to propose the clue of nanofluid. He debated that the combination of nanoparticles with base fluid improves the conductivity performance of the base fluid. Thermophoresis and Brownian motion expressions were offered by Buongiorno (2006). Barik and Dash (2014) considered the unsteady magnetohydrodynamics of a viscid, incompressible, electrically conducting fluid in a porous channel and concluded that the velocity at all points of the flow domain was subjugated due to the Hartmann number. Pattnaik *et al*. (2017) analysed wavering MHD free convection flow, heat and mass transfer flow through an exponentially accelerated inclined plate in a porous medium with homogeneous permeability. They concluded that the existence of a magnetic field and porous medium averts the flow swerve. Makinde and Aziz (2011) investigated the boundary layer flow impelled in a nanofluid as a result of a linearly stretching sheet and incorporated the effects of the Brownian motion and thermophoresis. They concluded that increasing the Brownian motion and thermophoresis reduces the Sherwood number. Many researchers discussed fluid flow in an inclined heated surface in various geometries. Some relevant literature can be seen through the investigations (Thiele and Knobloch, 2004; Kaboya *et al*., 2012; Makinde, 2007; Makinde, 2006a; Makinde, 2009) and several studies in their references.

The thermal system enhancement, as well as the energy usage during the flow system, is of vital interest to engineering processes. It is therefore important to look into the irreversibilities with regards to entropy generation rate. Entropy generation is the quantity of the damage of available work in the system; determining the entropy generation rate will, therefore, help in upgrading the system performance. With the pioneering work of Bejan (1979), several investigations on the entropy generation have been carried out by various scholars in numerous geometries. Makinde (2010) explored the thermodynamics second law dissection for gravity-driven flow for isothermal and isoflux heated slopping plates together with convective heat exchange at the free surfaces and concluded that the dominance effects of irreversibility fluid friction at the isothermal heated surface were highly felt. Eegunjobi and Makinde (2017) delved into communal effects of the magnetic field, thermal radiation, buoyancy forces and convective heat transfer on entropy generation in a mixed convection flow of an electrically conducting couple stress fluid through a vertical channel and concluded that magnetic field and thermal radiation exacerbated the entropy generation rate. Several studies on entropy generation on the flowing of fluid under diverse physical scenarios are found in the literature (Muhammad and Makinde, 2017; Monaledi and Makinde, 2018; Makinde, 2006b; Saouli and Aiboud-Saouli, 2004; Rosseland, 1936; Na,1979).

In this present study, we pay special attention to the effects of the fluid suction at the permeable inclined surface on irreversibility fraction and the entropy generation rate. In the succeeding sections, the physical problems representing the flow structures are formulated mathematically, analysed and solved. Substantial outcomes are presented in graphs and debated.

II. MATHEMATICAL FORMULATION

We examine the nonlinear flow of an electrically conducting and radiating chemically reacting nanoliquid film

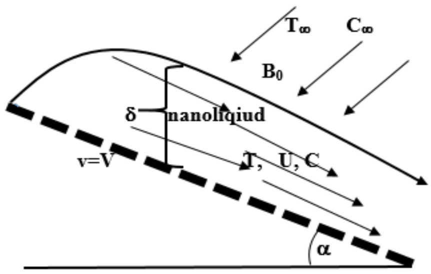

Figure 1. Problem geometry

over a permeable inclined isothermal or isoflux wall under the effect of a transversely imposed magnetic field as shown in Fig. 1. It is assumed that the fluid viscosity is a decreasing exponentially function of temperature and the discrepancy in the fluid density is due to temperature, nanoparticles concentration difference follows Bousinessq conjecture while the rest of the fluid properties remain constants.

Following (Kaboya *et al.*,2012; Makinde, 2006a; Makinde, 2010; Muhammad and Makinde, 2017), the temperature-dependent liquid film viscosity (μ) can be enunciated as

$$\mu = \mu_0 e^{-\gamma(T-T_\infty)} \tag{1}$$

where μ_0 means the dynamic viscosity at the ambient temperature T_∞, γ implies the viscosity variation parameter and T is the liquid film temperature. Following the Roseland approximation (Roseland,1936), the local radiative heat flux term for optically thick gray fluid is given by

$$q_r = -\frac{4\sigma^*}{3k^*}\frac{\partial T^4}{\partial y} \approx -\frac{16\sigma^* T_\infty^3}{3k^*}\frac{\partial T}{\partial y}, \tag{2}$$

where $T^4 \approx T_\infty^3 T - 3T_\infty^4$ (using Taylor approximation), k^* denotes mean absorption coefficient and σ^* is Stefan-Boltzmann constant. Therefore,

$$\frac{\partial q_r}{\partial y} \approx -\frac{16\sigma^* T_\infty^3}{3k^*}\frac{\partial^2 T}{\partial y^2}. \tag{3}$$

With the stated assumptions, the continuity, momentum, energy, concentration and volumetric entropy generation equations evolve (Thiele and Knobloch, 2004; Kaboya *et al*., 2012; Makinde, 2007; Makinde, 2006a; Makinde, 2009; Makinde, 2010; Makinde, 2006b; Saouli and Aiboud-Saouli, 2004).

$$\frac{\partial u}{\partial x} = 0, \tag{4}$$

$$\frac{d}{dy}\left(\mu\frac{du}{dy}\right) + \rho V\frac{du}{dy} - \sigma B_0^2 u + (\rho g\beta_1)(T-T_\infty)\sin\alpha \tag{5}$$
$$+(\rho g\beta_2)(C-C_\infty)\sin\alpha$$

$$\left(1+\frac{16\sigma^* T_\infty^3}{3kk^*}\right)\frac{d^2T}{dy^2} + \frac{\rho c_p V}{k}\frac{dT}{dy} + \frac{\mu}{k}\left(\frac{du}{dy}\right)^2 + \frac{\sigma B_0^2}{k}u^2 \tag{6}$$
$$\frac{\tau}{k}\left[D_B\frac{dT}{dy}\frac{dC}{dy} + \frac{D_T}{T_\infty}\left(\frac{dT}{dy}\right)^2\right] = 0,$$

$$D_B\frac{d^2C}{dy^2} + V\frac{dC}{dy} + \frac{D_T}{T_\infty}\frac{d^2T}{dy^2} - \varepsilon(C-C_\infty) = 0, \tag{7}$$

$$E_g = \frac{k}{(T_w-T_\infty)^2}\left(1+\frac{16\sigma^* T_\infty^3}{3kk^*}\right)\left(\frac{dT}{dy}\right)^2 + \frac{\mu}{(T_w-T_\infty)}\left(\frac{du}{dy}\right)^2 \tag{8}$$
$$+\frac{\sigma B_0^2 u^2}{(T_w-T_\infty)} + \frac{RD_B}{(T_w-T_\infty)}\frac{dT}{dy}\frac{dC}{dy} + \frac{RD_B}{(C_w-C_\infty)}\left(\frac{dC}{dy}\right)^2.$$

The boundary conditions for us to inspect at both isothermal and isoflux slanted wall surface are written as

$$u = \frac{\mu}{L}\frac{du}{dy},\ ak\frac{\partial T}{\partial y} = \frac{kb}{\delta}(T_w-T_\infty) - \frac{k}{\delta}(T_w-T_\infty) \tag{9}$$
$$D_B\frac{\partial C}{\partial y} = -\frac{D_T}{T_\infty}\frac{dT}{dy}, \quad \text{at} \quad y = 0.$$
$$\frac{du}{dy} = 0,\ -k\frac{\partial T}{\partial y} = h_f(T-T_\infty),\ C = C_\infty \ \text{at}\ y = \delta \tag{10}$$

where u represents axial velocity, $V(>0)$ is the fluid suction velocity at the permeable inclined surface, δ implies the thickness of liquid film, L stands for the slip length parameter, α portends angle of inclination, B_0 signify the uniform magnetic field acting perpendicular to the liquid film flow, T_w implies temperature at the wall, C denotes the nanoparticles concentration, the Brownian motion mass diffusivity is D_B, D_T presages the thermophoresis mass diffusivity, ε is the reaction rate, C_w is the plate surface nanoparticles concentration, C_∞ is the nanoparticles concentration at the liquid free surface, R is the universal gas constant, h_f represents heat transfer coefficient, k is the thermal conductivity, (x, y) are the axial and normal coordinates to the incline plane surface, c_p is the specific heat at constant pressure, ρ is the liquid film density, g is the gravitational acceleration, β_1 is the volumetric thermal expansion coefficient, β_2 is the concentration expansion coefficient, Eg is the entropy generation rate, while a and b are inclined wall heating parameters. Isoflux heating occurs where $a = 1$, $b = 0$ and isothermal heating take place where $a = 0$, $b = 1$. We introduce the following variables and parameters:

$$\eta = \frac{y}{\delta},\ \theta = \frac{T-T_\infty}{T_w-T_\infty},\ \phi = \frac{C-C_\infty}{C_w-C_\infty},\ W = \frac{u\delta}{\upsilon_0},\ \upsilon_0 = \frac{\mu_0}{\rho}, \tag{11}$$
$$\lambda = \gamma(T_w-T_\infty),\ M = \frac{\sigma B_0^2\delta^2}{\mu_0},\ Ra = \frac{g\beta_1(T_w-T_\infty)\delta^3}{\upsilon_0^2}$$
$$Bi = \frac{h_f\delta}{k},\ \mathrm{Nr} = \frac{16\sigma^* T_\infty^3}{3kk^*},\ S = \frac{\mu_0}{\delta L},\ \chi = \frac{\beta_2(C_w-C_\infty)}{\beta_1(T_w-T_\infty)},$$
$$\mathrm{Pr} = \frac{\mu_0 c_p}{k},\ Ec = \frac{\upsilon_0^2}{c_p\delta^2(T_w-T_\infty)},\ Ns = \frac{\infty\delta^2 E_g}{k},$$
$$Nb = \frac{\tau D_B(C_w-C_\infty)}{k},\ \mathrm{Re} = \frac{\rho V\delta}{\mu_0},\ Nt = \frac{\tau D_T(T_w-T_\infty)}{kT_\infty},$$
$$Sc = \frac{\upsilon_0}{D_B},\ \gamma = \frac{\varepsilon\delta^2}{\upsilon_0},\ n = \frac{RD_B(C_w-C_\infty)}{k}.$$

The unitless governing equations are attained as

$$\frac{d^2W(\eta)}{d\eta^2} - \lambda\frac{d\theta(\eta)}{d\eta}\frac{dW(\eta)}{d\eta} + \mathrm{Re}\frac{dW(\eta)}{d\eta}e^{\lambda\theta(\eta)} \tag{12}$$
$$-MW(\eta)e^{\lambda\theta(\eta)} + Ra[\theta(\eta) + \chi\phi(\eta)]e^{\lambda\theta(\eta)}\sin(\alpha) = 0,$$

$$(1+Nr)\frac{d^2\theta(\eta)}{d\eta^2} + \mathrm{RePr}\frac{dW(\eta)}{d\eta} + Ec\mathrm{Pr}\left(\frac{dW(\eta)}{d\eta}\right)^2 e^{-\lambda\theta(\eta)} \tag{13}$$
$$+Ec\mathrm{Pr}MW(\eta)^2 + Nb\frac{d\theta(\eta)}{d\eta}\frac{d\phi(\eta)}{d\eta} + Nt\left(\frac{d\theta(\eta)}{d\eta}\right)^2 = 0,$$

$$\frac{d^2\phi(\eta)}{d\eta^2} + Sc\mathrm{Re}\frac{d\phi(\eta)}{d\eta} + \frac{N_t}{N_b}\frac{d^2\theta(\eta)}{d\eta^2} - Sc\gamma\phi(\eta) = 0, \tag{14}$$

$$Ns = (1+Nr)\left(\frac{d\theta(\eta)}{d\eta}\right)^2 + Ec\mathrm{Pr}e^{-\lambda\theta(\eta)}\left(\frac{dW(\eta)}{d\eta}\right)^2 + \tag{15}$$
$$Ec\mathrm{Pr}MW(\eta)^2 + n\left[\frac{d\theta(\eta)}{d\eta}\frac{d\phi(\eta)}{d\eta} + \left(\frac{d\phi(\eta)}{d\eta}\right)^2\right].$$

with

at $\eta = 0$:

$$W = Se^{-\lambda\theta(\eta)}\frac{dW}{d\eta},\ a\frac{d\theta}{d\eta} = b\theta - 1,\ \frac{d\phi}{d\eta} = -\frac{Nt}{Nb}\frac{d\theta}{d\eta}, \tag{16}$$

and at $\eta = 1$:

$$\frac{dW}{d\eta} = 0,\ \frac{d\theta}{d\eta} = -Bi\,\theta,\ \phi = 0.$$

where Re (>0) is the fluid suction Reynolds number at the permeable inclined surface, Bi symbolizes Biot number, S is the slip parameter, Pr is the Prandtl number, Ec is the Eckert number, M is the magnetic field parameter,

Ra is the Rayleigh number, χ is the nanoparticles Buoyancy parameter, Sc is the Schmidt number, γ is the chemical reaction parameter, Nr is the radiation parameter, Nb is the Brownian motion parameter, Nt is the thermophoresis parameter, n is the nanoparticles irreversibility parameter, and λ is the variable viscosity parameter. Other parameters of interests are skin friction coefficients (C_f), Nusselt number (Nu), Sherwood number (Sh) and Bejan number (Be) defined as

$$C_f = \frac{\delta^2 \tau_w}{\rho v_0^2} = e^{-\lambda\theta} \frac{dW}{d\eta}\bigg|_{\eta=0}, \qquad (17)$$
$$Nu = \frac{\delta q_w}{k(T_w - T_\infty)} = -(1+Nr)\frac{d\theta}{d\eta}\bigg|_{\eta=0},$$
$$Sh = \frac{\delta q_m}{D_B(C_w - C_\infty)} = -\frac{d\phi}{d\eta}\bigg|_{\eta=0},$$
$$Be = \frac{N_1}{Ns} = \frac{1}{1+F}\bigg|,$$

where the wall shear stress τ_w, the wall heat flux q_w, the wall mass flux q_m and the irreversibility fraction F given as

$$\tau_w = \mu \frac{du}{dy}\bigg|_{y=0}, q_w = -k\left(1 + \frac{16\sigma^* T_\infty^3}{3kk^*}\right)\frac{dT}{dy}\bigg|_{y=0} \qquad (18)$$
$$q_m = -D_B \frac{dC}{dy}\bigg|_{y=0}, N_1 = (1+Nr)\left(\frac{d\theta(\eta)}{d\eta}\right)^2, F = \frac{N_2+N_3}{N_1},$$
$$N_2 = Ec\mathrm{Pr}e^{-\lambda\theta(\eta)}\left(\frac{dW(\eta)}{d\eta}\right)^2 + Ec\mathrm{Pr}MW(\eta)^2,$$
$$N_3 = \eta\left[\frac{d\theta(\eta)}{d\eta}\frac{d\phi(\eta)}{d\eta} + \left(\frac{d\phi(\eta)}{d\eta}\right)^2\right],$$

N_1 represents irreversibility due to heat transfer, N_2 denotes entropy generation due to viscous dissipation and N_3 is the irreversibility due to nanoparticles mass transfer rate.

III. NUMERICAL PROCEDURE

The nonlinear boundary value problem in Eqs. (12)-(14) along with the boundary conditions (16) are worked out numerically using a shooting manner coupled with the Runge-Kutta- Fehlberg integration scheme. The model equations are first transmuted to a set of non-linear first-order initial value problem. Let

$$W(\eta) = q_1, W'(\eta) = q_2 \qquad (19)$$
$$\theta(\eta) = q_3, \theta'(\eta) = q_4, \phi(\eta) = q_5, \phi'(\eta) = q_6.$$

The model Eqs. (12)-(14) then become

$$q'_2 = \lambda q_4 q_2 - \mathrm{Re} q_2 e^{\lambda q_3} + M q_1 e^{\lambda q_3} \qquad (20)$$
$$-(q_3 + \chi q_5) Ra\, e^{\lambda q_3}$$
$$q'_4 = -\frac{1}{1+Nr}\left(Ec\mathrm{Pr} q_2^2 e^{-\lambda q_3} + Ec\mathrm{Pr} M q_1^2\right) - \frac{1}{1+Nr}\left(\mathrm{RePr} q_4 + Nb q_3 q_6 + Nt q_4^2\right),$$
$$q'_6 = Sc\gamma q_5 - Sc\mathrm{Re} q_6 - \frac{Nt}{Nb} q'_4$$

with initial conditions as

$$q_1(0) = 0, q_2(0) = c_1, q_3(0) = 0, \qquad (21)$$
$$q_4(0) = c_2, q_5(0) = 0, q_6(0) = c_3$$

where c_1, c_2 and c_3 are guesses initial conditions and afterwards determine by shooting scheme using the iterative process. Then the resultant results have been integrated with the help of Runge-Kutta- Fehlberg procedure (Na, 1979).

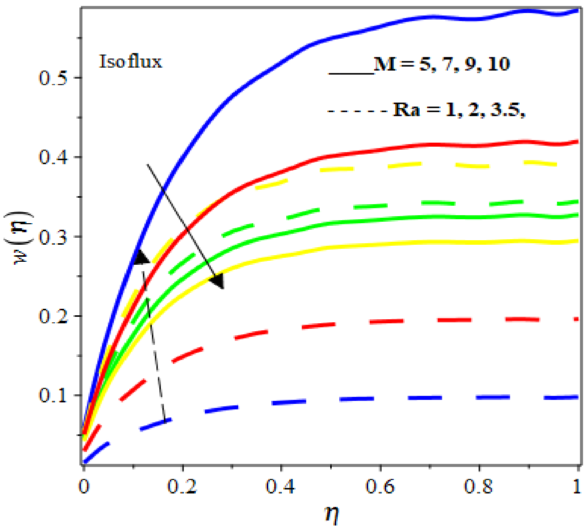

Fig. 2(a): Velocity profile with increasing M and Ra.

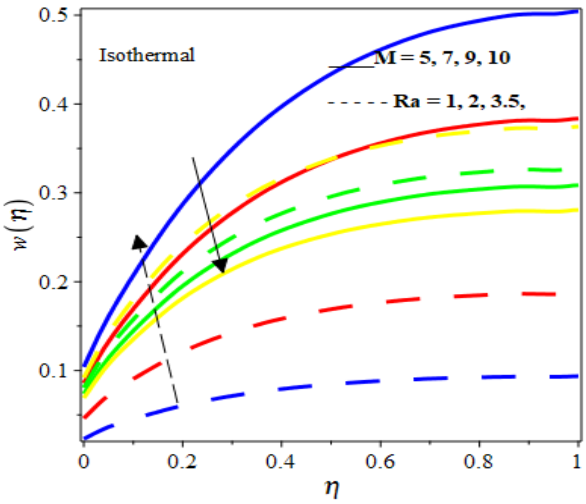

Fig. 2(b): Velocity profile with increasing $\boldsymbol{M}$ and $\boldsymbol{Ra}$.

IV. RESULTS AND DISCUSSION

Equations (12) to (14) along with Eq. (16) are solved numerically. The influences of magnetic field parameter (M), Rayleigh number (Ra), angle of inclination (α), suction Reynolds number (Re) and Radiating parameter parameter (Nr) on velocity (w), temperature (θ), entropy generation (Ns) and the Bejan number (Be) are explored and analysed through graphs (Figs 2-10) for the fixed values of other parameters. The effects of M, Ra, Re and α on velocity profile for both isothermal and isoflux walls are revealed in Figs. 2-3.

Figures 2(a)-(b) exhibit the influences of magnetic field parameter and Rayleigh number on the velocity description for both isothermal and isoflux walls. It is noticed from these figures that as the magnetic field parameter rises the velocity profile reduces. The reduction is more observed at the free surface than the suction wall. This is well seen in the velocity equation as the uniform magnetic field stand-in perpendicular to the liquid film flow. In these figures as well, we observed that heighten in the Rayleigh number escalates the velocity profile. The

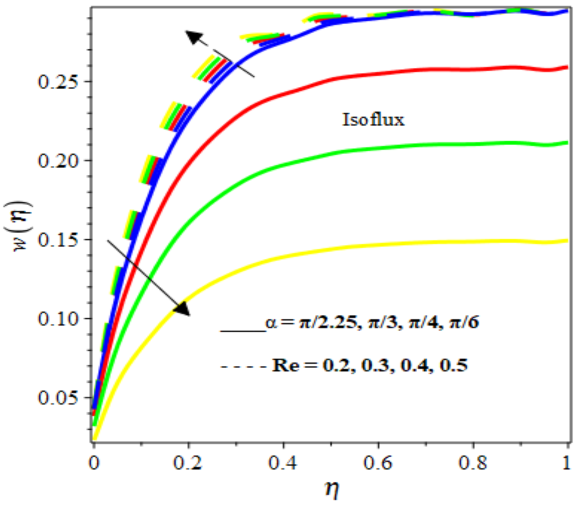

Fig.3(a): Velocity profile with increasing α and Re.

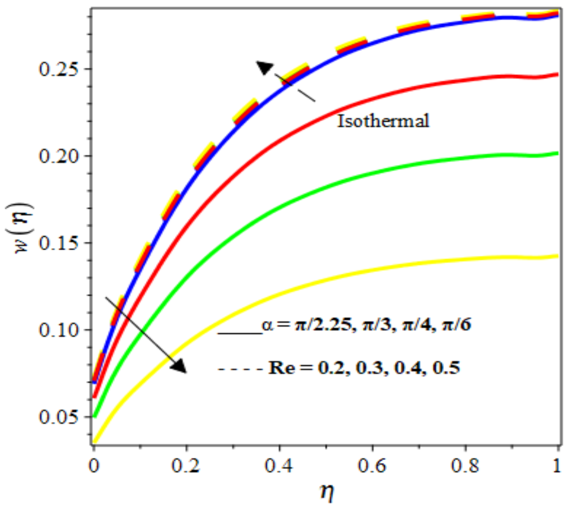

Fig. 3(b): Velocity profile with increasing α and Re.

increase is well noticed at the free surface wall. This escalation is expected since an increase in Rayleigh number tends to diminish in thermal layer thickness and therefore escalate the flow velocity. The behaviours of suction Reynold number and the angle of inclination on the velocity profile for both isothermal and isoflux are shown in Figs. 3 (a)-(b). From the displayed figures, it is perceived that the velocity profiles decline as the angle of inclination is decreasing for both isothermal and isoflux wall. This reduction is well noticeable at the free surface wall. The decrease in the velocity profiles may be ascribed to diminishing in the nanoparticle buoyancy parameter due to diminution in the angle of inclination. In the same figures, the effects of suction Reynolds number are shown. As seen in Eq. (12) and observed in the figures, an increase in the Reynolds number influences an increase in the velocity profiles for both walls.

Figures 4(a)-(b) evince the behaviours of magnetic field parameter and Rayleigh number on the temperature profiles for isothermal and isoflux walls. It is noticed in the figures that as the Rayleigh number is rising, the temperature profiles for these two walls escalate and unite at the suction wall for the case of isothermal. It is well

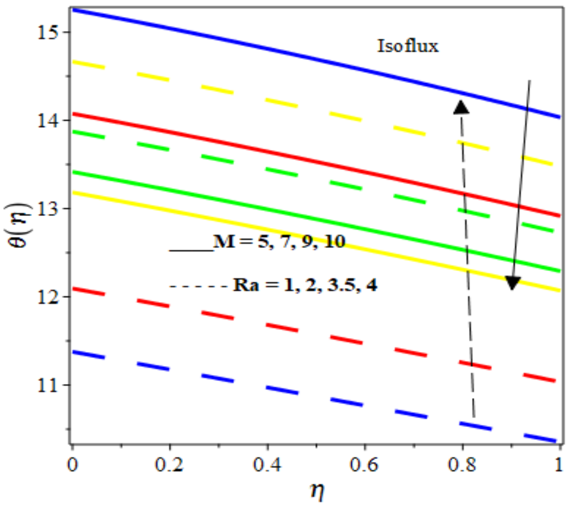

Fig. 4(a): Temperature profile with increasing M and Ra.

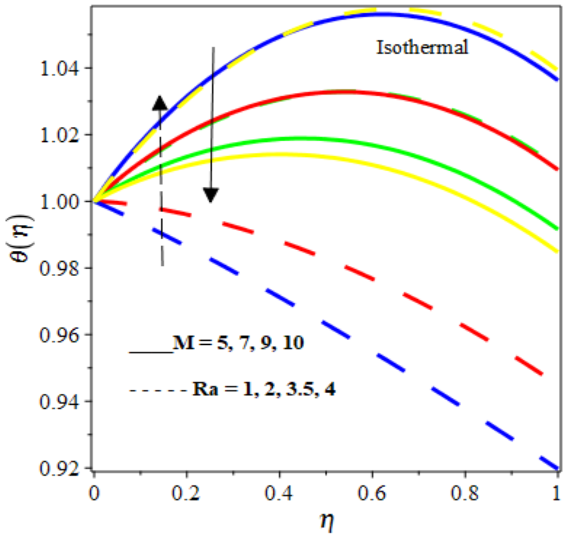

Fig. 4(b): Temperature profile with increasing M and Ra.

known that the Rayleigh number is the measure of fluid mass density which is caused by the temperature difference. In other words, the Rayleigh number is directly proportional to temperature discord. Intensifying the Rayleigh number will automatically tend to increase in the temperature. In Figs.4(a)-(b) as well, we observed the weights of the magnetic field parameter on the temperature profiles. It is unmasked that as the magnetic field parameter is intensifying, it slows down the temperature profiles. This might be ascribed to the appearance of restrictive Lorentz force. Figures5(a)-(b) are presented to demonstrate the influences of the angle of inclination and suction Reynolds number on the temperature profiles. For the two walls, it is observed that an increase in the suction Reynolds number tends to increase the temperature profiles. This is due to the fact that suction Reynolds number contains features such as density and viscosity which both fluctuate with temperature. The effects of inclined angle are presented in the same figures. It turned out that the profile of the temperature attained a higher value with a greater value of angle of inclination and a lower value with the smallest value of angle of inclination.

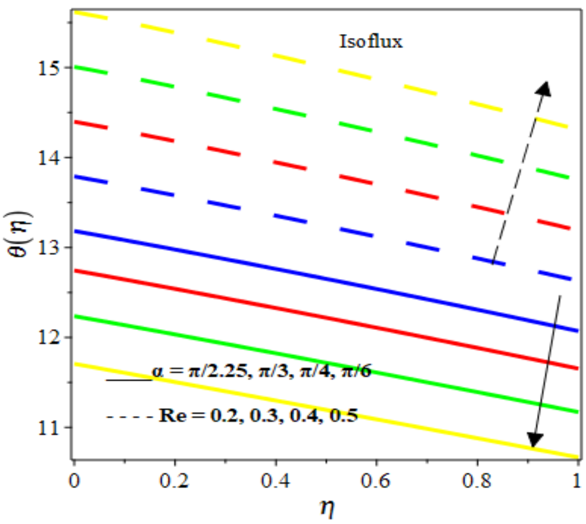

Fig.5(a): Temperature profile with increasing α and Re.

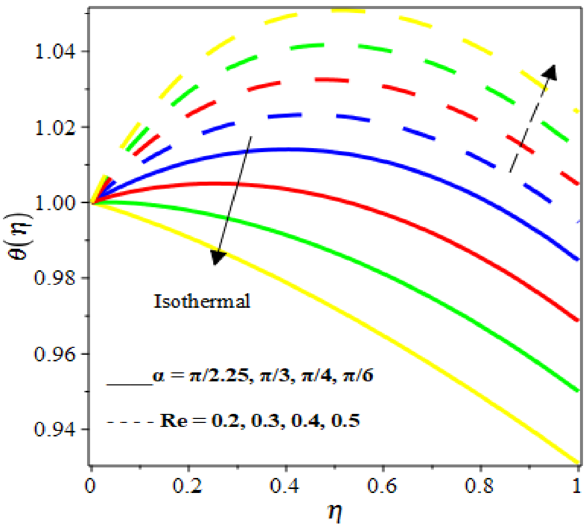

Fig. 5(b): Temperature profile with increasing α and Re.

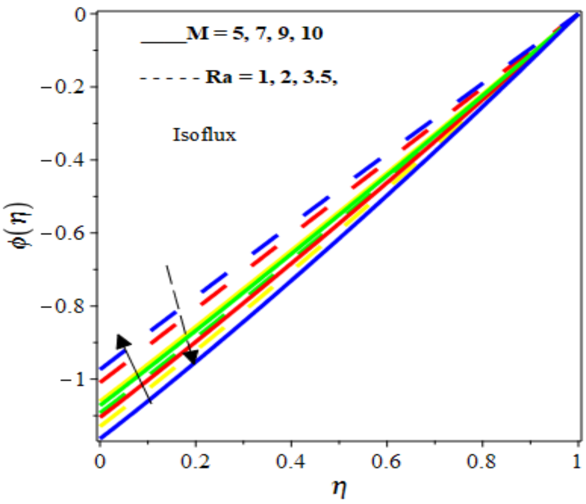

Fig. 6(a): Concentration profile with increasing M and Ra.

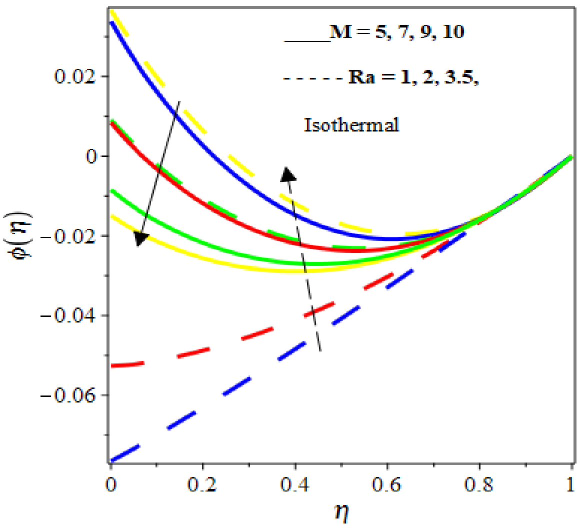

Fig. 6(b): Concentration profile with increasing M and Ra.

The behaviours of M, Ra, Re and α on the nanoparticle concentration profiles are demonstrated in Figs. 6 and 7. It is generally noted in these figures that the nanoparticle concentration unite at the frees surface wall for both isothermal and isoflux with respects to change of the governing parameters mentioned. It is noted in Fig. 6(a) that increasing magnetic field value tends to cause the thermal boundary layer nanoparticle concentration to be thicker and hence increase the nanoparticle concentration at the free suction wall but in Fig. 6(b), the increase in magnetic field value caused the thermal boundary layer thin, which therefore slow down the nanoparticle concentration at the free surface wall. Figure. 6(a)-(b) as well shown the impact of Rayleigh number on the nanoparticle concentration. It is observed in Fig. 6(a) that increasing the Rayleigh number, decrease the nanoparticle concentration. This might be ascribed to deterioration in the heat transfer while Fig.6(b) enhanced the nanoparticle concentration by increasing the Rayleigh number due to an improvement in heat transfer. Figures7(a)-(b) depicts the influences of suction Reynolds number on the concentration of the nanoparticle. It is observed in Fig.7(a) that the nanoparticle concentration reduces with increasing suction Reynold number. This reduction is due to diminishing in the heat transfer while Fig.7(b) shows that nanoparticle concentration rises with increasing the suction Reynold number. The decrease in inclination angle enhanced the concentration of the nanoparticle as shown in Fig.7(a) while it declined the concentration of the nanoparticle as shown in Fig.7(b).

The behaviours of M, Ra, Re and α on the entropy generation profiles are demonstrated in Figs. 8 and 9(a). The consequence of the imposed magnetic field of the flow structure on the entropy generation profile is demonstrated in Fig.8(a). we observed that increasing magnetic field parameter led to a reduction of the entropy generation rate this is as a result of heat transfer. The figure also alluded to the fact that as the Rayleigh number rise, it enhanced the fluid flow strength and also heat transfer and therefore improve the entropy generation rate. Figures 8(b) and 9(a) depict the influences of inclination angle and Reynold number on entropy generation rate. These figures show as the inclination angle is decreasing, there exist a decrement in the entropy generation rate. In the same figures as well, the influences of

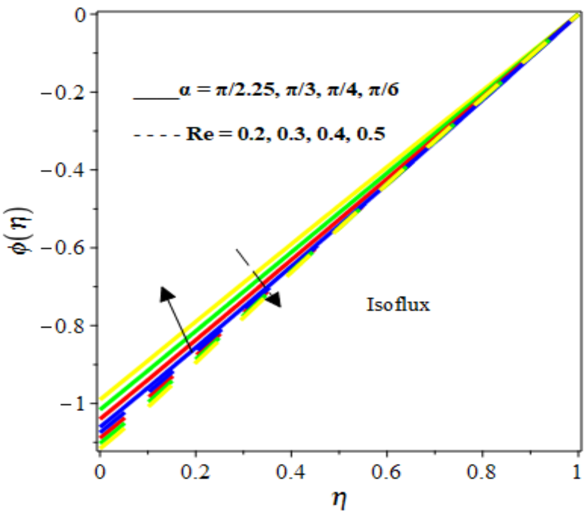

Fig. 7(a): Concentration profile with increasing α and Re.

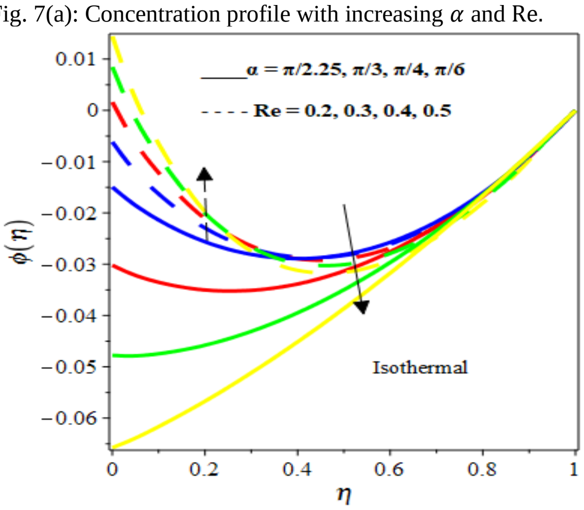

Fig. 7(b): Concentration profile with increasing α and Re.

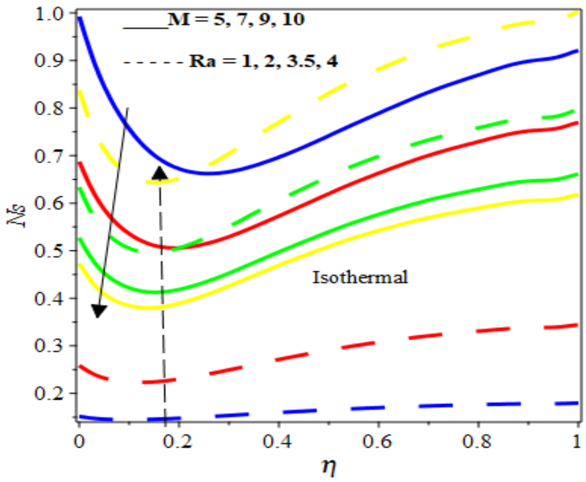

Fig. 8(a): Entropy profile with increasing M and Ra.

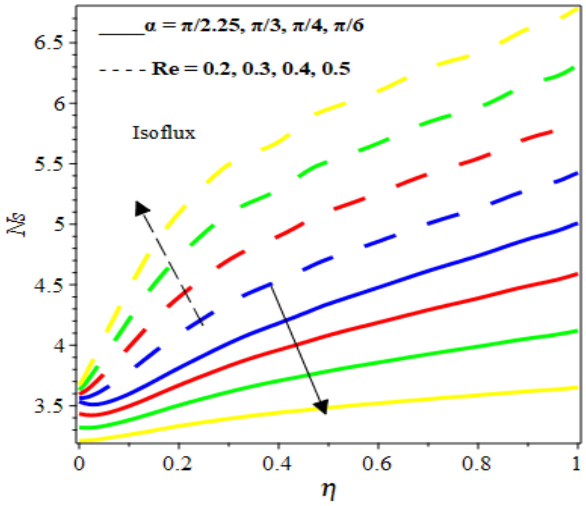

Fig. 8(b): Entropy profile with increasing α and Re.

suction Reynold number are shown. The suction Reynold number enhanced the input of entropy generation rate as a consequence of viscous dissipation, nanoparticle mass transfer rate and heat transfer in the boundary layer.

Figue 9(b) analyses the effects of magnetic field parameters and Rayleigh number on the Bejan number. Increasing magnetic field value as revealed in this figure, the Bejan number escalate across the system. This expresses that combined entropy generation caused by viscous dissipation and irreversibility caused by nanoparticles mass transfer rate dominates the flow system. With the same figure, the effect of Rayleigh number is shown. As the Rayleigh number value rises, the Bejan number dropdown. This indicates that irreversibility due to heat transfer prevails. The influences of inclination angle and the Reynold number are displayed in Figs.10(a)-(b). In the presented figures, we observed that escalating the inclination angle gives rise to the Bejan number. This results in the fact that combined entropy generation caused by viscous dissipation and irreversibility caused by nanoparticles mass transfer rate dominates. The same applied to the case of increasing the Rayleigh number in Fig. 10(a) but in Fig. 10(b), an increase in the Rayleigh number give rise to the Bejan number on the suction wall but does not affect the free surface wall. This means that the dominance effects of combined entropy generation ascribed to viscous dissipation and irreversibility ascribed to nanoparticles mass transfer rate happened on suction wall. The impact of the magnetic field, inclination angle and the Rayleigh number is depicted in Fig. 11. It is observed that the skin friction is improved with increasing the magnetic field parameter versus the Rayleigh number and decreases with increasing magnetic field parameter versus the inclination angle as shown in Fig.11(a). Meanwhile, Figs. 11(b) and 11(c) depict the impact of magnetic field intensity, Rayleigh number and inclination angle on the Nusselt number and Sherwood number. We noticed that as these are increasing, this enhanced the Nusselt number. Sherwood number decreases with increasing of the magnetic field parameter versus the inclination angle while increasing of the magnetic field parameter versus the Rayleigh number accelerate the Sherwood number

V. CONCLUSION

The inherent irreversibility in a hydromagnetic nanofluid flow along a permeable inclined surface with heat and mass transfer characteristics is numerically studied. Our results can be summarized as follows:

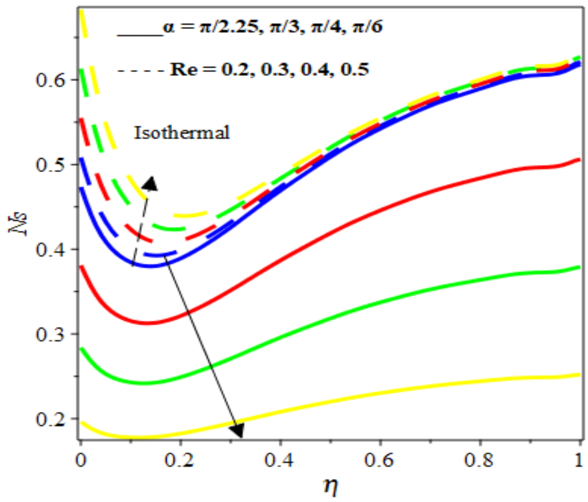

Fig. 9(a): Entropy profile with increasing α and Re.

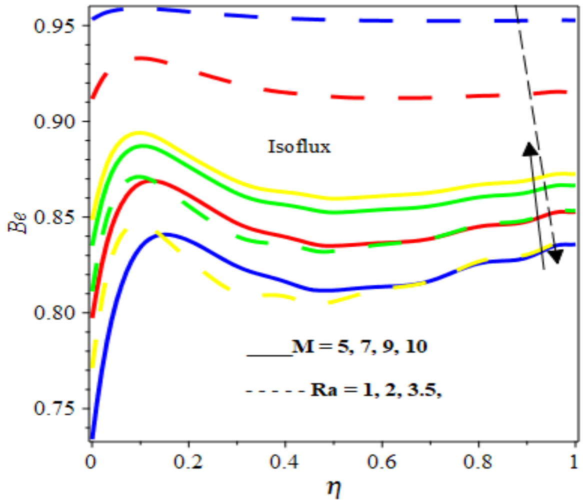

Fig. 9(b): The Benja with increasing M and Ra.

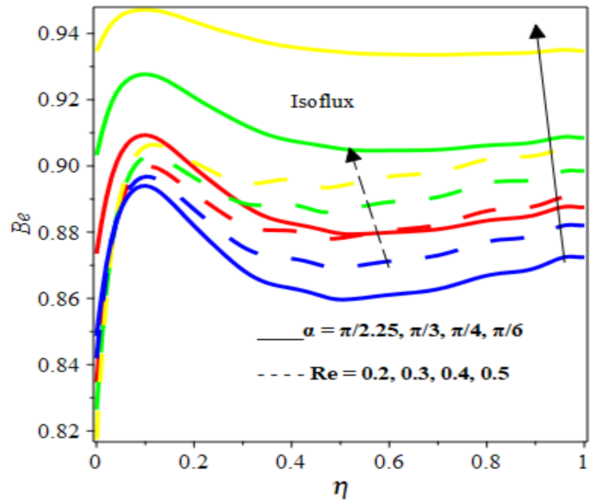

Fig. 10(a): The Benja with increasing α and Re.

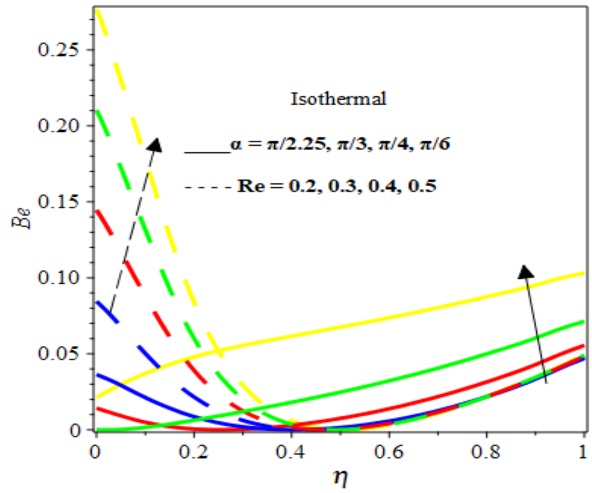

Fig. 10(b): The Benja with increasing α and Re.

- The velocity profile is a decreasing function of angle of inclination and magnetic field parameter while it increases by the Rayleigh number and the Reynold number.
- The temperature profile is a decreasing function of angle of inclination and magnetic field parameter while it increases by the Rayleigh number and the Reynold number.
- The nanoparticle concentration profile for isoflux wall is an increasing function of inclination angle and magnetic field parameter while it decreases by the Rayleigh number and the Reynold number.
- The nanoparticle concentration profile for isoflux wall is a decreasing function of inclination angle and magnetic field parameter while it increases by the Rayleigh number and the Reynold number.
- The entropy generation profile is a decreasing function of inclination angle and magnetic field parameter while it increases by the Rayleigh number and the Reynold number.
- The Bejan profile is an increasing function of inclination angle, the Reynold number and magnetic field parameter while it decreases by the Rayleigh number.
- The skin friction, Nusselt number and Sherwood number are enhanced with increasing the Rayleigh number.

REFERENCES

Barik, R.N. and Dash, G.C (2014) Thermal radiation effect on an unsteady magnetohydrodynamic flow past inclined porous heated plate in the presence of chemical reaction and viscous dissipation. *Applied Mathematics and Computation*. **226**,423–434.

Bejan, A. (1979) A study of entropy generation in fundamental convective heat transfer. *Journal of heat transfer*. **10**, 718-725.

Buongiorno, J. (2006) Convective transport in nanofluids, *ASME J. Heat Transf.* **128**, 240-250.

Choi, S.U.S. (1995) Enhancing thermal conductivity of fluids with nanoparticles *ASME Mech. Engng. Congress and Exposition*. San Franciscos, USA, **66**, 99–105.

Eegunjobi, A.S. and Makinde, O.D. (2017) Irreversibility analysis of hydromagnetic flow of couple stress fluid with radiative heat in a channel filled with a porous medium. *Results in Physics*. **7,** 459-469.

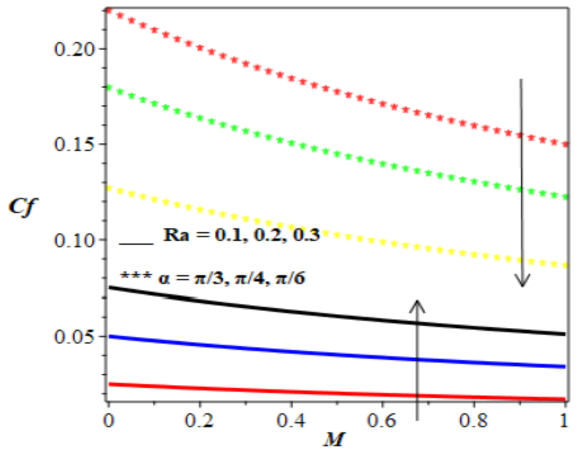

Fig. 11(a): Skin Frinction increasing M versus α and Ra.

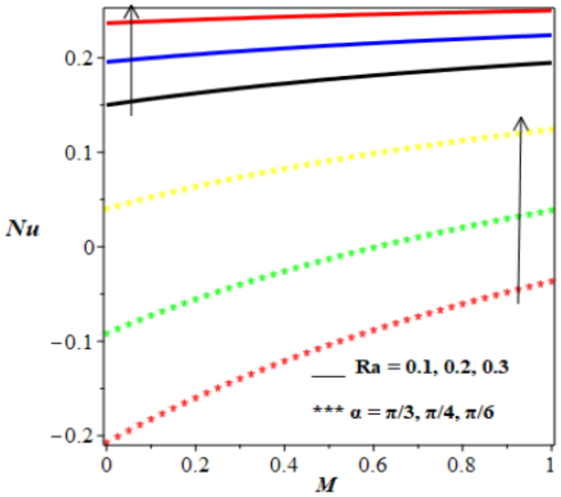

Fig. 11(b): Nusselt Frinction increasing M versus α and Ra.

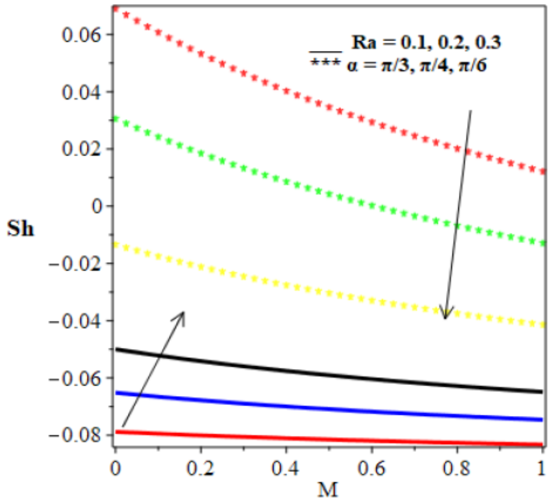

Fig. 11(c): Shewood Frinction increasing M versus α and Ra.

Kabova,Y.O., Kuznetsov, V.V., and Kabov, O.A. (2012) Temperature dependent viscosity and surface tension effects on deformations of non-isothermal falling liquid film. *International Journal of Heat and Mass Transfer*. **55**, 1271–1278.

Makinde, O.D. (2006a) Laminar falling liquid film with variable viscosity along an inclined heated plate. *Applied Mathematics and Computation*. **175**, 80-88.

Makinde, O.D. (2006b) Irreversibility analysis for gravity driven non-Newtonian liquid film along an inclined isothermal plate. *Physica Scripta*. **74**, 642-645.

Makinde,O.D. (2007) Hermite-Padé approximation approach to steady flow of a liquid film with adiabatic free surface along an inclined heat plate. *Physica A*. **381**, 1-7.

Makinde, O.D. (2009) Thermal criticality for a reactive gravity driven thin film flow of a third grade fluid with adiabatic free surface down an inclined plane. *Applied Mathematics and Mechanics*. **30**, 373-380.

Makinde,O.D. (2010) Thermodynamic second law analysis for a gravity-driven variable viscosity liquid film along an inclined heated plate with convective cooling. *Journal of Mechanical Science and Technology*. **24**, 899-908.

Makinde,O.D and Aziz, A. (2011) Boundary layer flow of a nanofluid past a stretching sheet with a convective boundary condition. *International Journal of Thermal Sciences*. **50**, 1326-1332.

Monaledi, R.L and Makinde, O.D. (2018) Entropy analysis of a radiating variable viscosity EG/Ag nanofluid flow in microchannels with buoyancy force and convective cooling. *Defect and Diffusion Forum*. **387**, 273–285.

Muhammad, A. and Makinde, O.D. (2017) Thermodynamics analysis of unsteady MHD mixed convection with slip and thermal radiation over a permeable surface. *Defect and Diffusion Forum*. **374**, 29-46.

Na,T.Y. (1979) *Computational methods in engineering boundary value problem*. Academic Press.

Pattnaik, J.R., Dash, G.C. and Singh, S. (2017) Radiation and mass transfer effects on MHD flow through porous medium past an exponentially accelerated inclined plate with variable temperature. *Ain Shams Engineering Journal*. **8**, 67–75.

Thiele, U. and E. Knobloch, E. (2004) Thin liquid films on a slightly inclined heated plate. *Physica D*. **190**, 213–248.

Rosseland, S. (1936) *Theoretical astrophysics*. Oxford University, New York, NY, USA.

Saouli, S. and Aiboud-Saouli, S. (2004) Second law analysis of laminar falling liquid film along an inclined heated plate. *Inter. Comm. Heat Mass Transfer*. **31**, 879-886.

Received: January 9, 2021
Sent to Subject Editor: January 15, 2021
Accepted: June 27, 2021
Recommended by Subject Editor Gianfranco Caruso